International Journal of Mechanical Sciences 140 (2018) 200–210

Contents lists available at ScienceDirect

International Journal of Mechanical Sciences

journal homepage: www.elsevier.com/locate/ijmecsci

Elastic imperfect tip-loaded cantilever cylinders of varying length

Jie Wang[1], Adam J. Sadowski[2,*]

Department of Civil and Environmental Engineering, Imperial College London, UK

ARTICLE INFO

Keywords:
Nonlinear mechanics
Cylindrical cantilever shells
Global transverse shear
Ovalisation
Imperfection sensitivity
Helical meshing

ABSTRACT

A number of recent publications have explored the crucial relationship between the length of a thin cylindrical shell and the influence of pre-buckling cross-sectional ovalisation on its nonlinear elastic buckling capacity under bending. However, the research thus far appears to have focused almost exclusively on uniform bending, with ovalisation under moment gradients largely neglected.

This paper presents a comprehensive computational investigation into the nonlinear elastic buckling response of perfect and imperfect thin cantilever cylinders under global transverse shear. A complete range of practical lengths was investigated, from short cylinders which fail by shear buckling to very long ones which exhibit local meridional compression buckling with significant prior cross-section ovalisation. Two imperfection forms were applied depending on the length of the cylinder: the linear buckling eigenmode for short cylinders and a realistic weld depression imperfection for long cylinders. The weld depression imperfection was placed at the location where the cross-section of the perfect cylinder was found to undergo peak ovalisation under transverse shear, a location that approaches the base support with increasing length. Compact closed-form algebraic expressions are proposed to characterise the elastic buckling and ovalisation behaviour conservatively, suitable for direct application as design equations.

This study contributes to complete the understanding of cylindrical structures of varying length where the dominant load case is global transverse shear, including multi-strake aerospace shells with short individual segments between stiffeners and long near-cylindrical wind-turbine support towers and chimneys under wind or seismic action.

1. Introduction

A cylinder under global transverse shear is a classical structural system that finds application in containment vessels under seismic excitation, aerospace fuselages under transverse vibrations and chimneys or wind turbines under wind or seismic loads. Early algebraic treatments such those of Lu [1] and Schröder [2] demonstrated that the relative proximity of the smooth circumferentially-sinusoidal membrane stress state under global transverse shear to the simple membrane stress states of uniform torsion or uniform meridional compression allowed these to be used to establish closed-form 'first approximations' for the critical buckling stress of short and long cylinders respectively. These have served as the basis for most design expressions ever since. However, the unsymmetrical response makes more accurate investigations, such as those exploring the geometrically nonlinear phenomenon of ovalisation in long cylinders, prohibitively complex to perform algebraically and recourse must be made to computational methods. For example, the recent computational study of Rotter et al. [3] on cylinders under *uniform* bending confirmed and extended on earlier algebraic studies that ovalisation only begins to significantly reduce the nonlinear elastic buckling resistance in cylinders longer than $\omega \approx 0.5(r/t)$ or $\Omega \approx 0.5$ [4], where ω and Ω are dimensionless length parameters defined by:

$$\omega = \frac{L}{r}\sqrt{\frac{r}{t}} = \frac{L}{\sqrt{rt}} \text{ and } \Omega = \frac{L}{r}\sqrt{\frac{t}{r}} \text{ such that } \omega = \frac{r}{t}\Omega \tag{1}$$

Here L, r and t are the cylinder length, radius and thickness respectively. These dimensionless groups will be used widely in what follows. Ovalisation was found to lead to a 'fully-developed' reduction in the elastic buckling strength of approximately 50% by $\Omega \approx 5$, becoming largely invariant with increases in length beyond $\Omega \approx 7$. The apparent 'ovalisation boundary' of $\Omega \approx 0.5$ is probably a *lower* bound for cylinders under transverse shear, as the presence of a moment gradient will reduce the intensity of the bending along the cylinder length and attenuate the extent of pre-buckling flattening.

* Corresponding author.
E-mail address: a.sadowski@imperial.ac.uk (A.J. Sadowski).
[1] Post-Doctoral Researcher in Structural Engineering
[2] Lecturer in Structural Engineering

https://doi.org/10.1016/j.ijmecsci.2018.02.027
Received 4 January 2018; Received in revised form 9 February 2018; Accepted 10 February 2018
Available online 15 February 2018

The focus in the literature on laboratory testing has historically been on rather short shells (typical length to radius L/r ratio of 1) intended for use as fuselages, reactors or containment structures in the aerospace, nuclear and civil engineering industries respectively. In the early experiments of Lundquist [5] on ~100 aluminium alloy cylinders under global transverse shear and bending, all specimens were of a length that was within an approximate range $10 < \omega < 50$ or $0.025 < \Omega < 0.12$. The polyester cylinders of Yamaki [6] also occupied a length range $10 < \omega < 50$ or $0.025 < \Omega < 0.12$, the mild steel specimens of Galletly and Błachut [7] occupied $10 < \omega < 15$ or $0.05 < \Omega < 0.11$, the nickel-plated shells of Michel et al. [8] all had $\omega \approx 21.2$ and $\Omega \approx 0.05$, while the stainless-steel cylinders of Athiannan and Palaninathan [9] fell in $16 < \omega < 21$ or $0.048 < \Omega < 0.06$. Schmidt and Winterstetter [10] reported on transverse shear tests performed on a cylinder composed of three laser-welded segments of different thickness. Each segment exhibited a length of $\omega \approx 40$ or $\Omega \approx 0.04$, such that the full cylinder was still quite short at $\omega \approx 120$ or $\Omega \approx 0.12$. Where a focus on imperfections was part of the test programme, every study concluded that these short cylinders under shear were relatively insensitive to them due to a stable post-buckling equilibrium path.

Computational studies that were performed in cylinders under transverse shear were done usually as a supplement to test programmes, and thus they too focused on short cylinders that buckled into a shear mode. Kokubo et al. [11] was perhaps the first to perform a parametric finite element study of this system, including both linear buckling eigenvalue and geometrically and materially nonlinear path-tracing analyses with various eigenmode-affine imperfections using custom-written software. A significantly milder imperfection sensitivity was found when compared to that of a cylinder under uniform meridional compression, with a reduction in buckling load of ~20% at an imperfection amplitude of 3 wall thicknesses under shear (as opposed to ~80% under compression [12]). The more recent modelling of Gettel and Schneider [13] appears to be one of the few to have investigated longer cylinders up to $\omega \approx 1060$ or $\Omega \approx 2.1$ computationally, also including an in-depth discussion on the appropriate choice of suitable imperfections in light of the novel provisions of the then recently-published European Standard on metal shells EN 1993-1-6 [14]. However, the paper does not discuss ovalisation, which for cylinders of length $\Omega \approx 2.1$ would be expected to cause up to a 30–40% reduction in the elastic critical buckling moment if subject to uniform bending [3]. The authors are aware only of the earlier work of Schneider and Thiele [15] where ovalisation in long transversely-loaded cylinders (up to $\Omega \approx 5.2$) was illustrated explicitly, and it is telling that the title of their paper begins with the words 'an unexpected failure mode'.

The authors are not aware of any tests to investigate the elastic ovalisation response of very long cylinders under global shear, presumably due to the expense and practicalities involved in handling tall vertical specimens in a laboratory. Yamaki's [6] polyester specimens would have to have been one metre tall to achieve $\Omega = 0.5$, and over ten metres tall to approach fully-developed ovalisation at $\Omega > 5$. However, since structures such as slender metal wind turbine towers may routinely reach dimensions exceeding $\Omega = 6$ [16], it is important for this reference result to be part of modern engineering knowledge. The reader is warmly invited to consult the comprehensive reviews of historical literature on cylindrical forms under global shear in Athiannan and Palaninathan [9], Schmidt and Winterstetter [10] and Michel et al. [17] for further valuable background information.

2. Scope of the study

A comprehensive parametric investigation into the influence of the full range of practical lengths, slendernesses and different types of imperfection form on the nonlinear elastic stability of cantilever cylinders under global transverse shear does not appear to have ever been performed. In the authors' opinion, this is likely due to restrictions in the computing power available to previous research programmes. Additionally, previous results were presented mostly in a graphical format which makes them rather difficult to generalise, and a compact algebraic characterisation in terms of appropriate dimensionless groups also does not appear to have been performed. This study exploits the great advances in personal computing made in recent decades to conduct over one thousand finite element simulations in a relatively short timescale, approximately one month on a single workstation, aided by the model management and automation methodology detailed in Sadowski et al. [18]. The analyses performed included (with computational analysis acronyms as defined by EN 1993-1-6 [14]):

- Linear bifurcation analyses (LBAs) on ~50 different lengths from $\omega = 3$ (very short) to $\Omega = 10$ (very long) for r/t ratios of 50, 100, 200, 300, 500 and 1000.
- Geometrically nonlinear analyses of the perfect elastic cylinder (GNAs) on ~50 different lengths from $\omega = 3$ to $\Omega = 50$ for r/t ratios of 50, 100, 200 and 500.
- Geometrically nonlinear analyses of imperfect elastic cylinders (GNIAs) on approximately 60 different lengths from $\omega = 3$ to $\Omega = 20$ for a single r/t of 100, divided between two qualitatively different geometric imperfection forms (more details below). Equivalent total geometric deviations δ_e/t of 0.1, 0.25, 0.5, 0.75, 1, 1.5 and 2 were investigated for both forms.

The parameter ranges given above were chosen with the intent of addressing the main practical applications, from short containment structures to long supporting structures. The choice of two different imperfection forms was made to relate them to the expected nonlinear response of the shell in different length domains, similar in concept to 'quasi-collapse-affine imperfections' discussed by Gettel and Schneider [13]. For shorter cylinders dominated by shear buckling, the computed critical linear bifurcation (LBA) eigenmode was used as an imperfection form due to its affinity with the nonlinear buckling mode. However, for longer cylinders dominated by local meridional compression buckling and ovalisation, a single instance of the weld depression imperfection of Rotter and Teng [12] was placed at the location of peak cross-sectional ovalisation where the flattening of the wall (and thus the reduction in the critical buckling stress) was found to be greatest. This imperfection form has been widely used in computational studies of cylinders under compression [19] and uniform bending [20,21], and is considered a realistic representation of a common manufacturing defect in longer welded shells [22]. The nominal imperfection amplitudes δ_0 for the above two geometric forms were re-cast into 'equivalent geometric deviations' δ_e to account for the fact that the nominal amplitude of an eigenmode wave is only half of the total geometric deviation that the shell is subject to (see further details in Fajuyitan et al. [23]). A corresponding investigation into the elastic-plastic response at varying lengths lies beyond the scope of this paper and will be presented at a later time. The outcomes of the simulations are presented here in terms of resistances at the buckling limit state, intended for interpretation within the Reference Resistance Design framework [18,24,25]. Further details of the modelling procedure are given in the following section.

3. Computational modelling and validation

3.1. Mesh design

The analyses were performed using the ABAQUS 6.14-2 [26] finite element software with special care paid to mesh design, as illustrated schematically in Fig. 1. The double-helix partitioning procedure of Sadowski and Rotter [27] was applied to generate inclined meshes for the analysis of short cylinders where the dominant failure mode was buckling under shear. These authors had shown that a 'regular' mesh of quadrilateral shell elements aligned with the axis of the cylinder was in conflict with the preferred orientation of a shear buckle under pure torsion, leading to a slow rate of convergence and an overly stiff response because the quadrilateral shell elements were themselves subject

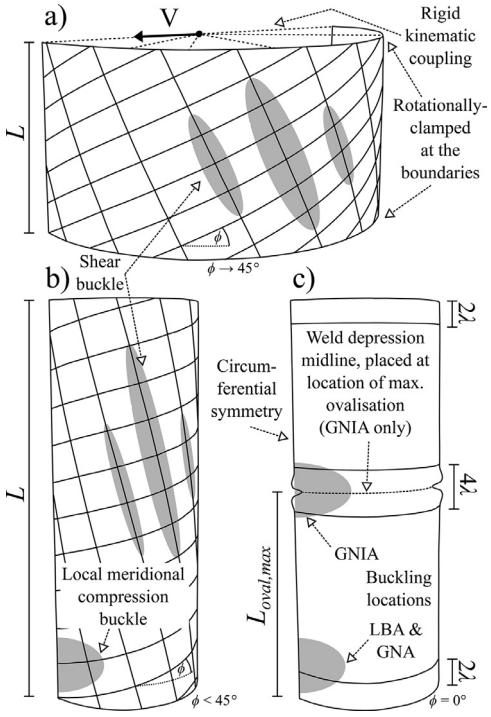

Fig. 1. Model partition design for 'helical' and 'regular' meshes: a) short cylinders buckling predominantly in shear; b) longer cylinders with interactive buckling modes and c) long cylinders exhibiting meridional compression buckling with ovalisation.

to shear. However, a 'helical' mesh inclined at close to 45° showed no such numerical penalty because the orientation of the mesh was aligned with that of the buckle and the elements were under biaxial action.

A preliminary set of LBAs was performed in the range $3 \le \omega \le 50$ to establish an appropriate angle of inclination ϕ to the circumferential axis (Fig. 1) of the partition that would generate a 'helical' mesh that is sympathetic to the orientation of the buckling mode. Approximated by Eq. (2), this expression suggests that shear buckles are inclined at close to 45° for very short cylinders (Fig. 1a), akin to under pure torsion, whereas they become increasingly vertical for longer cylinders ($\phi \to 0$ as $\omega \to \infty$; Fig. 1b). For lengths beyond $\omega = 50$, it will be shown that local buckling near the base under meridional compression takes over as the critical mode (and for $\phi < \sim 15°$ a helical mesh anyway becomes oriented very closely to the cylinder axes), and a 'regular' rectangular mesh was applied instead (Fig. 1c). This partitioning and meshing scheme was used for all analyses: LBAs, GNAs and GNIAs. The authors appear to be the first to apply custom helical meshing for the accurate analysis of shear buckling in short cylinders, with previous studies all using regular rectangular meshing schemes [8,11,15,28,29].

$$\phi \approx \begin{cases} 45 & \omega \le 3 \\ 45\left(1 - e^{-2.3(\omega-5)^{-0.45}}\right) & 3 < \omega < 50 \end{cases} \begin{pmatrix} \phi \text{ in degrees} \to \text{ the} \\ \text{circumferential axis} \end{pmatrix} \quad (2)$$

An element size of between 2% to 10% of the linear bending half-wavelength $\lambda \approx 2.44\sqrt{(rt)}$ was applied uniformly in 'helical' meshes to accurately capture the large shear buckling modes. However, 'regular' meshes were refined in regions within 2λ of the bottom and top cylinder boundaries to enable an accurate modelling of local compatibility bending at these locations, and also within 2λ of the midline of a weld depression imperfection, if applied (Fig. 1c). Between these regions, a coarser but smoothly-graded mesh was used. The computationally-efficient reduced-integration S4R thick shell element was used throughout, and a single plane of circumferential symmetry was exploited for further efficiency. A transverse force V was applied via a reference point placed at the centroid of the loaded diametral plane, rigidly linked to the edge of the shell. Rotationally-clamped boundary conditions were simulated at both ends, though the loaded end was free to displace transversely and meridionally. The material of the shell was taken as simple isotropic steel with $E = 200$ GPa and $\nu = 0.3$ in the full parametric analyses, and for GNAs and GNIAs the Riks modified arc-length algorithm was used.

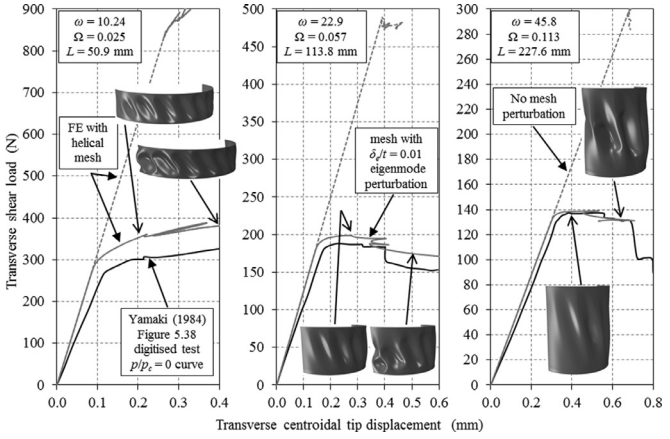

Fig. 2. Finite element predictions and test results for the elastic buckling of short polyester cylinders under transverse shear (test data for cylinder digitised from Fig. 5.38 of Yamaki [6]), $E = 5.56$ GPa, $\nu = 0.3$, $r = 100$ mm and $t = 0.247$ mm ($r/t \approx 405$).

3.2. Validation against the test results of Yamaki (1984)

A number of analyses were first performed to validate the helically-meshed finite element model for short cylinders for which test data was available. Yamaki [6] had performed a series of global transverse shear tests on pressurised cylinders made of polyester film (Young's modulus $E = 5.56$ GPa and Poisson ratio $\nu = 0.3$) that were so thin ($r/t \approx 405$ with $t = 0.247$ mm) as to buckle elastically. While cylinders of different lengths were tested by Yamaki, they all occupied a dimensionless length range of $10 < \omega < 50$ or $0.025 < \Omega < 0.12$ and thus initially failed by shear buckling, although an interaction with the local meridional compression mode was found to emerge later in the equilibrium path (Fig. 2).

A finite element simulation of a near-perfect cylinder (including a minor eigenmode-affine mesh perturbation of total amplitude 1% of the wall thickness) shows a very good agreement with Yamaki's test result (Fig. 2). The prediction is slightly stiffer than the test response due to the tested cylinders being inevitably affected by minor geometric imperfections or other misalignments, which are unknowable at this time, but the modelled perturbation amplitude could always be fine-tuned to obtain a closer agreement. It is shown that *some* mesh perturbation is crucial to enable the cylinder to pass smoothly into a deformed configuration associated with a shear buckling mode, as otherwise the cylinder proceeds along the linear fundamental path and significantly overestimates the response. A similar conclusion was reached by Kokubo et al. [11]. Lastly, there are no tests known to the authors of cylinders under transverse shear that would be sufficiently long to fail by local meridional compression buckling or to develop ovalisation, the predictions in what follow for longer cylinders will wherever possible be compared against known algebraic formulae for uniform bending.

4. Linear elastic buckling behaviour

Cylinders under global transverse shear are prone to buckling into different modes depending on the length. Shear buckling dominates in shorter, while meridional buckling controls in longer ones, with a short transitional region in between. The linear elastic buckling behaviour is exposed in detail in this section, first through a simple algebraic treat-

ment using shell membrane theory and then by more accurate finite element LBAs. In what follows, V_{cl} represents a reference classical elastic critical buckling load according to simple shell membrane theory while V_{LBA} represents a more accurate computational prediction of this resistance. V_{cr} is used to represent an *algebraic* approximation of V_{LBA} and uses the simple V_{cl} expression as a 'scaffold' upon which enhancements are appended based on the computational results.

4.1. Reference resistance V_{cl} from shell membrane theory

Under a transverse shear force V [F] applied at the cylinder tip ($z = L$), the membrane stress state in a cylindrical shell supported at $z = 0$ is given by:

$$N_\theta(z,\theta) = 0 \tag{3}$$

$$N_{z\theta}(z,\theta) = N_{z\theta,\max}\sin\theta \text{ where } N_{z\theta,\max} = \tau_{\max}\cdot t = \frac{V}{\pi r} \tag{4}$$

$$N_z(z,\theta) = N_{z,\max}\cos\theta \text{ where } N_{z,\max} = \sigma_{z,\max}\cdot t = \frac{V(z-L)}{\pi r^2} \tag{5}$$

where N_θ, $N_{z\theta}$ and N_z are the circumferential, shear and meridional membrane stress resultants [F.L^{-1}] respectively (σ and τ are the corresponding stresses in [F.L^{-2}]), while z and θ are the meridional (base support at $z = 0$) and circumferential (compressed side at $\theta = 0$) coordinates respectively. Ignoring boundary effects, the classical elastic critical buckling values for these stress resultants, derived under the reference conditions of uniform torsion and meridional compression respectively, are [14]:

$$N_{z\theta,\mathrm{cl}} = 0.75Et\left(\frac{t}{r}\right)\sqrt[4]{\frac{rt}{L^2}} \tag{6}$$

$$N_{z,\mathrm{cl}} = 0.605Et\left(\frac{t}{r}\right) \tag{7}$$

The dimensionless length approximating the boundary between the two buckling modes may be estimated by equating $N_{z\theta,max} / N_{z\theta,cl} = N_{z,max} / N_{z,cl}$ as:

$$\omega_{z\theta-z} \approx 0.65\frac{r}{t} \text{ or } \Omega_{z\theta-z} \approx 0.65 \tag{8}$$

The reference classical elastic critical buckling resistance V_{cl} for a cylinder under global transverse shear is thus here taken as:

$$V_{cl} = \begin{cases} V_{z\theta,cl} = 0.75\pi Et^2\sqrt[4]{\dfrac{rt}{L^2}} \text{ for } \omega \le \omega_{z\theta-z} \\ V_{z,cl} = 0.605\pi Et^2 \text{ for } \omega > \omega_{z\theta-z} \end{cases} \tag{9}$$

It should be emphasised that these simple expressions naturally cannot account for the effects of boundary restraint on the buckling mode, interaction between buckling modes, geometric nonlinearity or imperfections.

4.2. Reference resistances V_{LBA} and V_{cr} from finite element analysis

The first algebraic eigenvalue prediction of the elastic critical buckling load for cylinders of varying length under transverse shear appears to have been performed by Schröder [2] using Donnell shell theory which assumed a pure pre-buckling membrane stress state. His results were presented in the form $N_{max} / N_{z,cl}$ vs L/r, where N_{max} is the maximum meridional membrane stress at the lowest eigenvalue, and as they have been reproduced elsewhere [10] they are compared here against the nearest equivalent, $V_{LBA} / V_{z,cl}$, in Fig. 3. The agreement is remarkably close for short cylinders, although the algebraic prediction somewhat underestimates the buckling resistance in the shear mode. However, the rather approximate boundary between shear and meridional compression buckling suggested by Schröder [2] appears to be very conservative and not at all accurate. The LBA predictions also suggest that there is a *finite* (although short-lived) length range over which the shell exhibits an interaction between shear and meridional compression modes.

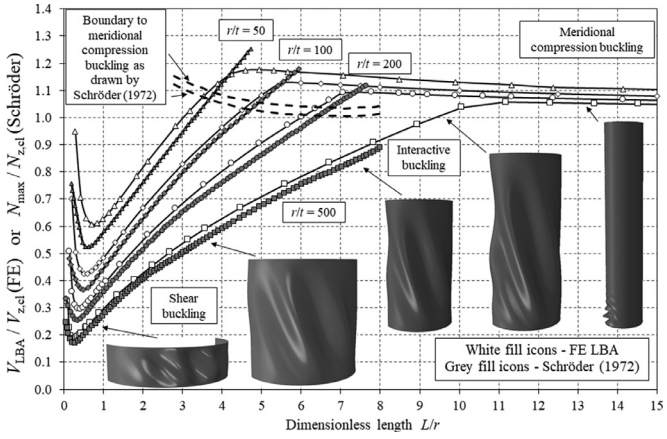

Fig. 3. Comparison of finite element LBAs against algebraic eigenvalue predictions (data digitised from Fig. 3 of Schröder [2]) of the linear elastic buckling of cylinders of varying length under transverse shear.

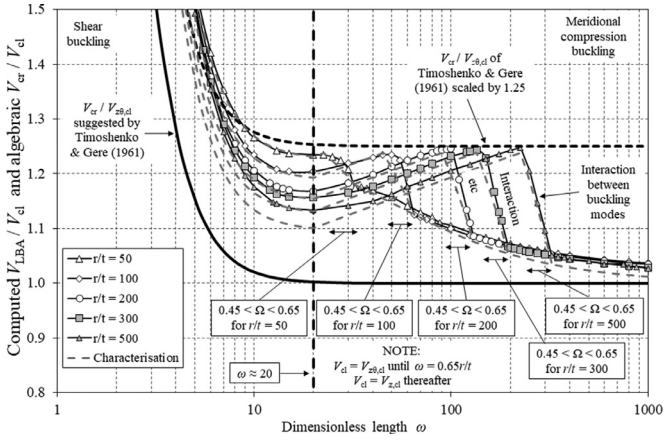

Fig. 4. Computed LBAs vs dimensionless length ω with algebraic characterisation.

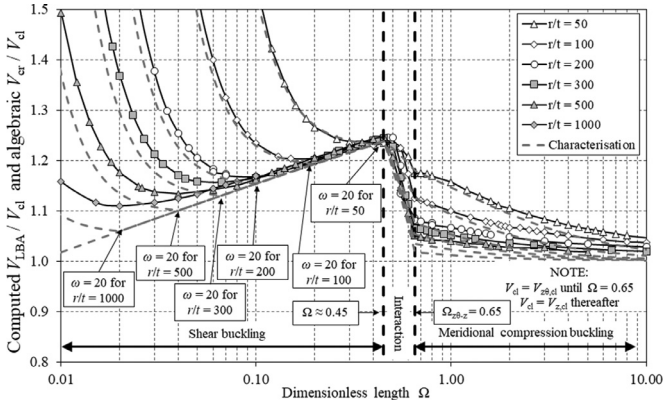

Fig. 5. Computed LBAs vs dimensionless length Ω with algebraic characterisation.

A more complete picture is obtained by reformulating the LBA predictions separately in terms of both dimensionless length groups ω and Ω (Eq. (1)), as shown in Figs. 4 and 5 respectively. It is stressed that in both figures, the normalisation of the vertical axis is done using $V_{z\theta,cl}$ until $\omega_{z\theta\text{-}z} = 0.65r/t$ or $\Omega_{z\theta\text{-}z} = 0.65$ and $V_{z,cl}$ for all lengths thereafter (Eq. (9)) to account for the qualitatively different buckling modes

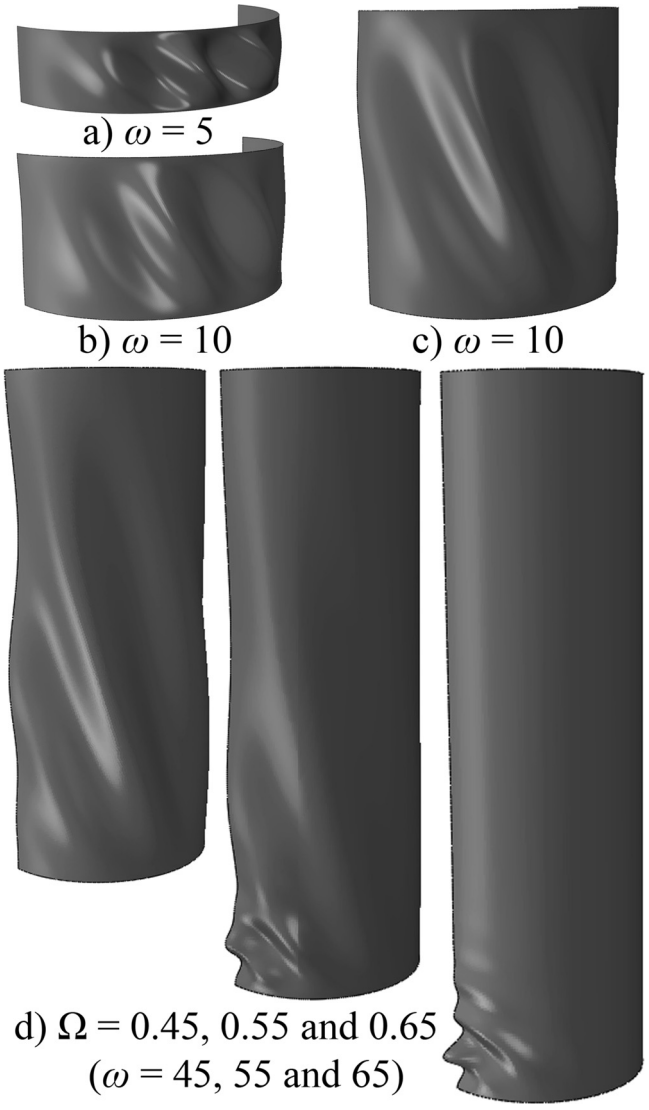

Fig. 6. Computed LBA modes at varying length for $r/t = 100$.

governing the behaviour in different length ranges. Four distinct length domains may be identified. Cylinders shorter than $\omega \approx 20$ buckle at an increasingly higher load V as $\omega \to 0$ due to the increasing restraint against shear buckling offered by the clamped boundary conditions. A similar effect was recently documented for very short cylinders under global bending [3,23]. There is a slight dependency on the r/t ratio in this length domain, with a thicker shell (lower r/t) requiring a higher buckling load to overcome the increasingly important through-thickness shear deformations, an effect captured by the finite element calculation but naturally not by a simple algebraic analysis. Cylinders longer than $\omega \approx 20$ but shorter than $\omega \approx 0.45r/t$ or $\Omega \approx 0.45$ buckle into an increasingly vertical shear mode (Eq. (2) and Fig. 6a–c) and see a modest rise in the buckling load relative to $V_{z\theta,cl}$ with increasing length. This simple algebraic expression (Eq. (6)) is derived from the condition of uniform torsion which assumes shear buckles at 45° to the horizontal. Buckling into steeper shear modes requires slightly more strain energy, a constraint responsible for the small rise in V_{LBA} relative to $V_{z\theta,cl}$.

Michel et al. [17] suggested that the following equation by Timoshenko and Gere [30], derived to account for boundary effects in short cylinders under uniform torsion and yielding a very similar result to the corresponding EN 1993-1-6 [14] equation, was an acceptable approximation under transverse shear:

$$\frac{V_{cr}}{V_{z\theta,cl}} = \frac{\tau_{cr}}{\tau_{z\theta,cl}} = \frac{N_{z\theta,cr}}{N_{z\theta,cl}} = 6.427\sqrt{\frac{1+0.0239\omega^3}{\omega^3}} \approx \sqrt{1+\frac{42}{\omega^3}} \tag{10}$$

It is shown here that this equation in fact leads to a significant underestimate of the theoretical elastic buckling load under transverse shear, as the V_{LBA} predictions under transverse shear are all consistently above any V_{cl} prediction established on the basis of the critical buckling stress under pure torsion, from a ~5% excess at $r/t = 1000$ to ~25% excess at $r/t = 50$. Lundquist [5] had apparently recognised this as early as 1935, suggesting a scaling factor of 1.25 on the prediction based on the critical stress under uniform torsion, shown in Fig. 4 to be somewhat closer to the more accurate LBA prediction.

The length domain of interaction between the shear and meridional compression linear buckling modes is visible most clearly in terms of Ω in Fig. 5, where a sudden drop in the buckling load relative to $V_{z\theta,cl}$ occurs inside the range ~0.45 < Ω < ~0.65. Here, the LBA mode exhibits features from both buckling forms (Fig. 6d), although the domain is rather short-lived (i.e. dΩ = 0.65 – 0.45 = 0.2 corresponds to only 2 or 6.3 mm for a shell with $r/t = 100$ or 1000 respectively and $t = 1$ mm). However, the upper boundary of this interaction domain is in surprisingly close agreement with the very simple prediction for $\Omega_{z,\theta\text{-}z} = 0.65$ in Eq. (8) established on the basis of simple membrane theory. This is because the critical meridional buckling stress established under uniform compression (Eq. (7)) *is* an accurate metric of buckling wherever a region of meridional compression is sufficiently wide to support a small buckle [3,31], regardless of the validity of using the critical shear buckling stress established under uniform torsion (Eq. (6)) for transverse shear. For all cylinders with Ω > 0.65, the base of the cylinder develops small and closely-spaced local meridional compression buckles and $V_{LBA} \to V_{z,cl}$ as $\Omega \to \infty$. The slight excess on $V_{z,cl}$ at the start of this 'long' domain, higher for thicker shells, is largely due to the restraint against buckling offered by the clamped conditions at the base of the cylinder. It should be stressed that the LBA prediction is unaffected by ovalisation, and it will *always* predict the compressed base of the cylinder as the critical location for buckling under transverse shear in long cylinders. This observation will become significant in the GNIA calculations later.

The authors propose the following algebraic characterisation (Eq. (11)) for the complete linear elastic buckling behaviour of this system across the full practical range of lengths and r/t ratios, qualitatively capturing shear, interactive and meridional compression buckling. It is illustrated in grey dashed lines on Figs. 4 and 5, where it may be seen that it offers a most accurate prediction relative to the LBAs as $r/t \to 50$ but an increasingly conservative one as $r/t \to 1000$. The inconsistency should be understood in the context of the difficulty in condensing this relationship into compact closed-form equations.

$$V_{cr} = \begin{cases} C_1\sqrt{1+\dfrac{70}{\omega^3}}\cdot V_{z\theta,cl} & \omega < 20 \\ \left(\dfrac{1.87}{1+0.46\Omega^{-0.13}}\right)\cdot V_{z\theta,cl} & 20\left(\dfrac{t}{r}\right) \le \Omega < 0.45 \\ 5(0.65C_2 - 0.45C_3 & 0.45 \le \Omega < 0.65 \quad \text{where} \\ \quad +(C_3 - C_2)\Omega)\cdot V_{z\theta,cl} & \\ \left(1.22 - 0.22e^{-\dfrac{55}{\omega}}\right)\cdot V_{z,cl} & \omega \ge 0.65\left(\dfrac{r}{t}\right) \end{cases}$$

$$C_1 = \left(\frac{1.86}{1+0.46(20t/r)^{-0.13}}\right) C_2 = \left(\frac{1.87}{1+0.46(0.45)^{-0.13}}\right) \approx 1.24$$

$$C_3 = \left(1.22 - 0.22e^{-85\left(\frac{t}{r}\right)}\right) \tag{11}$$

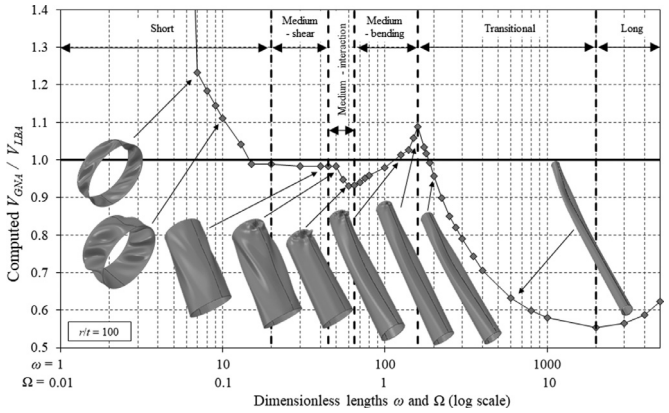

Fig. 7. Computed relationship between the critical transverse load V_{GNA} / V_{LBA} and the dimensionless lengths ω and Ω for a perfect cantilever cylinder with $r/t = 100$.

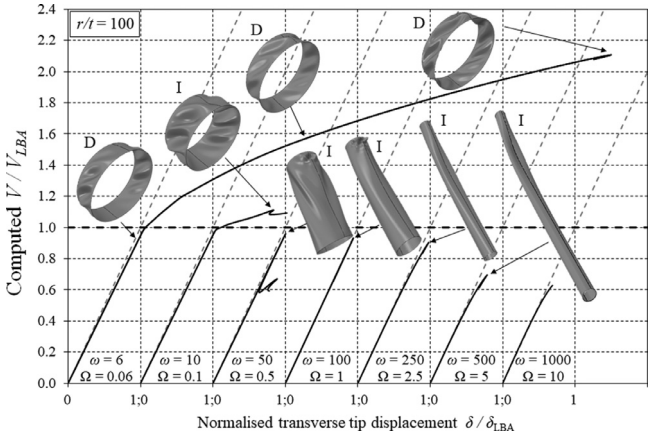

Fig. 8. Dimensionless transverse load-tip displacement curves for cylinders of different lengths with $r/t = 100$ ('D' and 'I' represent a deformed shape and an incremental buckling mode respectively).

5. Nonlinear behaviour of perfect elastic cantilever cylinders

Under geometrically nonlinear conditions, elastic cylinders under uniform bending are known to experience a complex interaction between cross-sectional ovalisation, local buckling, boundary effects and length [3]. The moment gradient of a cantilever system inevitably adds further complexity, and this is explored here through a comprehensive programme of GNAs. In what follows, V_{GNA} represents the prediction of the critical transverse shear buckling load from a GNA, while $V_{k,per}$ represents an approximation to this obtained solely by means of closed-form algebraic equations proposed by the authors. V_{LBA}, V_{cl} and V_{cr} have the same meaning as before. While this choice of notation may perhaps be disputed, it was chosen for clarity and convenience.

The relationship between the computed normalised value V_{GNA} / V_{LBA} and both dimensionless lengths ω and Ω is introduced in Fig. 7 for a perfect elastic cylinder with $r/t = 100$. A selection of corresponding GNA equilibrium paths are shown in Fig. 8, expressed as the relationship between the applied transverse shear load V, normalised by the LBA prediction V_{LBA}, and the tip centroidal displacement δ, normalised by its value at the LBA buckling load δ_{LBA} obtained using Timoshenko [32] beam theory (Eq. (12); with shear coefficient taken from Cowper [33]). The cylinder under global transverse shear appears to exhibit *six* distinct domains of behaviour controlled by the cylinder length, in contrast to four domains for cylinders under uniform bending [3] and only three domains for cylinders under the fundamental load cases of uniform meridional compression, external pressure or torsion

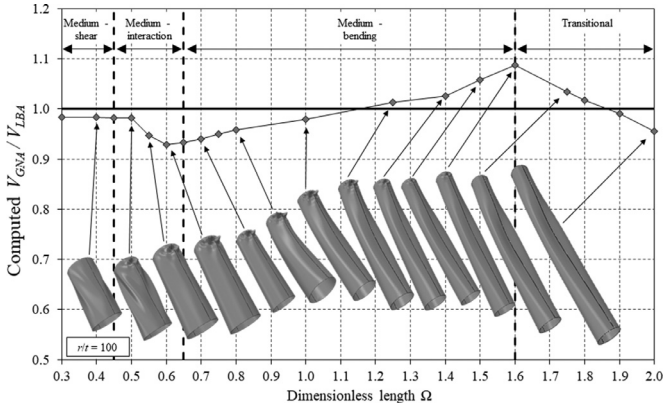

Fig. 9. Close-up of the relationship between the critical transverse V_{GNA} / V_{LBA} and the dimensionless cylinder length Ω for a perfect cylinder with $r/t = 100$ in the 'medium-bending' length domain. The shapes shown are incremental buckling modes.

[34].

$$\delta_{LBA} = \frac{V_{LBA}L^3}{3EI} + \frac{V_{LBA}L}{\kappa AG} \text{ where } \kappa = \frac{2(1+\nu)}{4+3\nu} \approx 0.53 \text{ and } G = \frac{E}{2(1+\nu)} \quad (12)$$

When the shell is very short, the free development of the shear buckling mode is restrained by the clamped edge boundaries and a transverse load significantly higher than $V_{z\theta,cl}$ is required to cause buckling. While this effect was also seen under linear conditions (Figs. 4 and 5), it is even more pronounced under geometrically nonlinear conditions with the elastic shell able to sustain very large amplified displacements and excesses on V_{LBA} prior to a buckling event at a load V_{GNA} (Fig. 8). In fact, although these very short shells develop significant deformations associated with a shear mode they eventually undergo bifurcation buckling into a local meridional compression mode, a behaviour that was also seen in Yamaki's experiments (Fig. 2). This domain is here termed 'short', and appears to persist for shells up to a length of $\omega \approx 20$, consistent with the characterisation under geometrically linear conditions (Fig. 4; Eq. (11)).

Cylinders longer than $\omega \approx 20$ but shorter than $\Omega \approx 0.45$ ($\omega \approx 0.45r/t$) are free to buckle unhindered into a shear mode, as evident by $V_{GNA} \approx V_{LBA}$ in this length range (where V_{LBA} also corresponds to a shear buckling mode; Figs. 5 and 6), and this length domain is here termed 'medium-shear'. Longer cylinders in the range $\sim 0.45 < \Omega < \sim 0.65$ (here termed the 'medium-interaction' length domain) exhibit an interaction between the shear and local meridional compression buckling modes, and a slight reduction in V_{GNA} relative to V_{LBA}. By $\Omega \approx 0.65$, the shear mode plays no further role in the buckling behaviour which is instead initially controlled by local buckling at the base of the compressed side of the cylinder (the 'medium-bending' length domain). This behaviour is in close agreement qualitatively and quantitatively to the linear buckling predictions from both LBA and classical algebraic analyses (Fig. 5; Eqs. (8) and (9)).

A detailed close-up of the behaviour in the 'medium-bending' domain is offered in Fig. 9. Assumed here to occupy a length range of $\sim 0.65 < \Omega < \sim 1.6$, this domain is long enough for ovalisation to potentially begin altering the behaviour (known to initiate at $\Omega > 0.5$ for uniform bending [3]). It may be seen in from the incremental buckling modes in this length range (obtained by subtracting the set of computed displacements immediately before the buckling event those immediately after it [35]) that flattening of the cylinder cross-section at approximately midspan begins to feature increasingly prominently as $\Omega \rightarrow \sim 1.6$. Simultaneously, the critical location for buckling gradually ceases to be the base of the most compressed side of the cylinder and instead shifts to the cylinder midspan where ovalisation is greatest. This

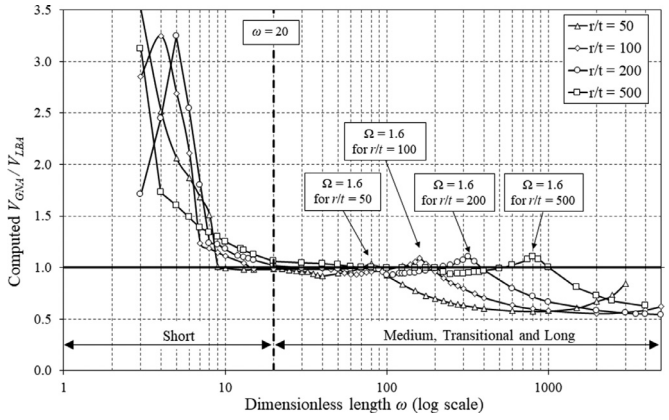

Fig. 10. Computed relationship between the nonlinear elastic buckling resistance V_{GNA} / V_{LBA} of perfect cantilever cylinders and the dimensionless length ω.

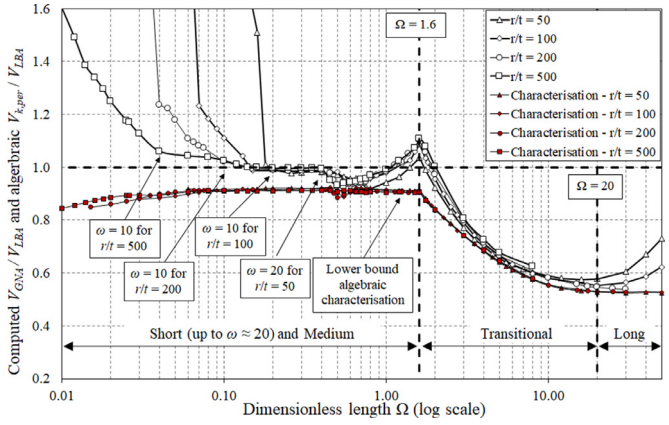

Fig. 11. Computed relationship between the nonlinear elastic buckling resistance V_{GNA} / V_{LBA} of perfect cantilever cylinders and the dimensionless length Ω.

interaction appears to constrain the buckling mode slightly, as evident by the transition being accompanied by a slight rise in V_{GNA} / V_{LBA} up to a ratio of approximately 1.1 (note that, for Ω > ~0.65, V_{LBA} always corresponds to a local meridional compression buckling mode at the base of the cylinder; Figs. 5 and 6).

For cylinders longer than Ω ≈ 1.6, buckling will always occur at the most flattened location (initially at midspan) and at a buckling load V_{GNA} / V_{LBA} that now begins to significantly decrease with increasing length to a minimum ratio of approximately ~0.55 at Ω ≈ 20 (Fig. 7) as pre-buckling ovalisation becomes more severe. The corresponding equilibrium paths in Fig. 8 show an increasingly nonlinear upper portion of the curve preceding bifurcation buckling. This length domain is here termed the 'transitional' one, in a direct parallel to the corresponding length domain under uniform bending [3]. This 'transitional' domain spans dΩ = 20 – 1.6 = 18.4, corresponding to a length range of 18.4 m or 581.9 m for a shell with t= 1 mm and r/t= 100 and 1000 respectively, and is thus likely to encompass a wide range of practical applications. Cantilever cylinders longer than Ω ≈ 20 are here classified as 'long'. The preceding relationships between V_{GNA} / V_{LBA} and length are illustrated for a wider range of r/t= 50, 100, 200 and 500 in Figs. 10 and 11 in terms of dimensionless groups ω and Ω respectively, showing that the length domains identified are qualitatively independent of the r/t ratio when the relationship is grouped in terms of ω and Ω as necessary.

The behaviour of 'long' cylinders (Ω > ~ 20) deserves further explanation. The computed relationships show a *rise* in the V_{GNA} / V_{LBA} ratio with increasing length beyond Ω ≈ 20. This is because the lever

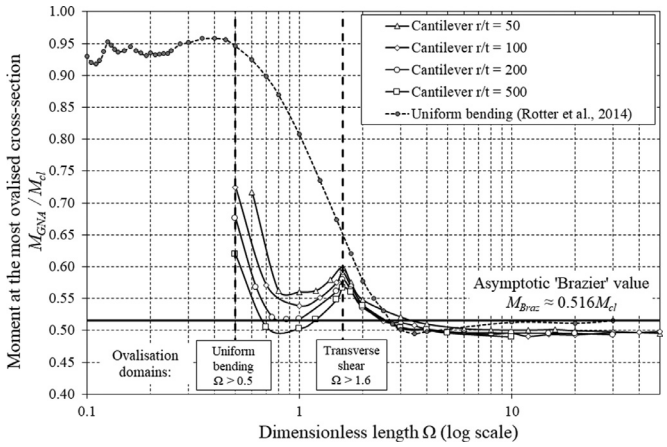

Fig. 12. Moment at the most ovalised cross-section in cantilever cylinders, compared with those under uniform bending from Rotter et al. [3].

arm of the transverse tip load becomes reduced as a very long cylinder undergoes significant tip deflections, and thus a higher load is required to achieve buckling at the fully-ovalised cross-section which in fact occurs at a moment very close to the Brazier [36] prediction M_{Braz} (Eq. (12)). This moment is itself only approximately 0.516 times the classical elastic critical buckling moment M_{cl} (Eq. (13)) which assumes local meridional compression buckling occurs when the stress resultant at the most compressed fibre reaches the $N_{z,cl}$ value and an undeformed geometry (Eq. (7)). This effect is illustrated in Fig. 12 where it may be seen that, although V_{GNA} / V_{LBA} increases for Ω > ~ 20 without bound (such very long cylinders lead to ill-conditioned finite element models that are difficult to run successfully), the actual moment at the most ovalised cross-section M_{GNA} / M_{cl} remains stable at a value approximately 5% below the M_{Braz} due to local buckling on the compressed side always preceding limit point buckling due to ovalisation [31,37]. Ovalisation is explored further in the next section.

$$M_{Braz} = \frac{2\sqrt{2}}{9}\left(\frac{E\pi rt^2}{\sqrt{1-\nu^2}}\right) \approx 1.035Ert^2 \tag{12}$$

$$M_{cl} = \pi r^2 N_{z,cl} \approx 1.901Ert^2 \tag{13}$$

The authors propose the following very simple but conservative algebraic characterisation of this complex nonlinear relationship, to be used in tandem with the set of equations proposed for V_{cr} (which approximate V_{LBA}) in Eq. (11):

$$\frac{V_{k,per}}{V_{cr}} = \begin{cases} 0.92 & \Omega < 1.6 \\ 0.92e^{-0.42(\Omega-1.6)^{0.85}} + 0.538\left(1 - e^{-0.42(\Omega-1.6)^{0.85}}\right) & \Omega \geq 1.6 \end{cases} \tag{14}$$

This relationship assigned a conservative 'plateau' value of 0.92 for the 'short' and 'medium' domains up to Ω = 1.6, neglecting the beneficial restraining effect offered by the boundary condition. Cylinders longer than Ω = 1.6 duly exhibit a reduction in the buckling load with length, attaining a 'plateau' value of V_{GNA} / V_{LBA} ≈ 0.538 at Ω > 20 and conservatively neglecting the rise in buckling load due to a reducing lever arm. The proposed functional form aims to strike a balance between usability and realism, and the numerical values may easily be adjusted if desired.

6. Quantification of ovalisation in cylinders under transverse shear

Xu et al. [31] illustrated computationally that circular cylinders under uniform bending develop peak cross-sectional ovalisation at or close to midspan, and there is little ambiguity as to the critical location for

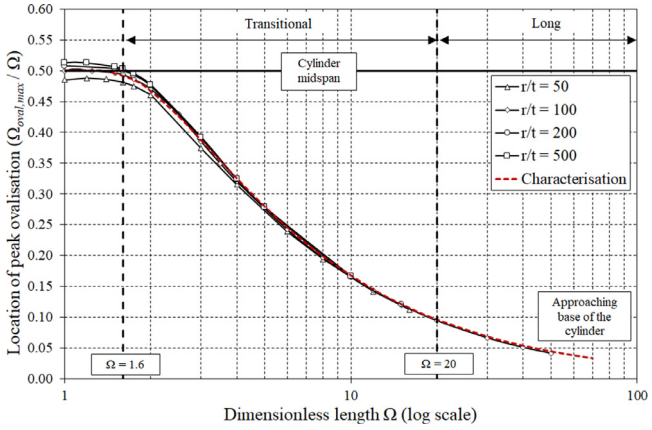

Fig. 13. Variation of $\Omega_{oval,max}$ / Ω, the ratio of the location of peak ovalisation to the total cylinder length.

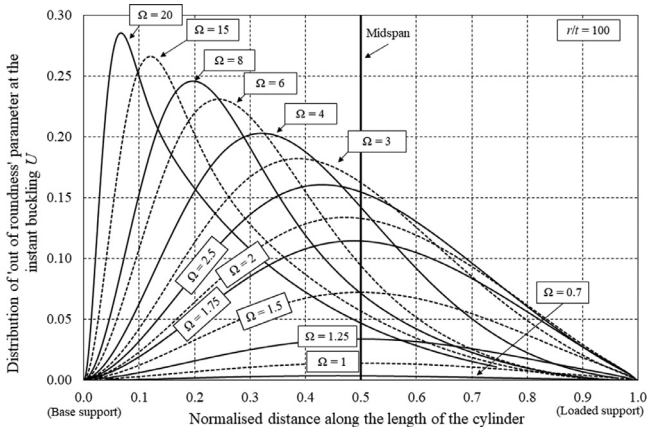

Fig. 14. Distribution of the 'out of roundness' parameter U at buckling with along the normalised cylinder length for cylinders of different length Ω but constant r/t= 100.

local meridional compression buckling. Under transverse shear, however, the moment gradient leads to a non-uniform distribution of flattening along the length, and the critical location for buckling in cylinders longer than the 'medium-bending' domain (Ω > ~1.6) is no longer obvious. The dimensionless location of the location of the most flattened cross-section along the cylinder, here termed $\Omega_{oval,max}$, relative to the total cylinder length Ω is illustrated in Fig. 13 as function of Ω. Only cylinders with Ω > 1 are shown, as those shorter than this experience negligible ovalisation, even when buckling into a shear mode. While the most ovalised location is initially approximately at midspan ($\Omega_{oval,max}$ / Ω ≈ 0.5), for longer cylinders this location approaches the base support ($\Omega_{oval,max}$ / Ω → 0) as, consequently, does the critical location for local meridional compression buckling. This phenomenon is characterised by the simple relationship in Eq. (15) and will be invoked in the final part of this paper in a study of imperfection sensitivity.

$$\frac{\Omega_{oval,max}}{\Omega} = \frac{L_{oval,\max}}{L} \approx \begin{cases} 0.5 & \Omega < 1 \\ 0.5\left(1 - e^{-2.7(\Omega-1)^{0.86}}\right) & \Omega \geq 1 \end{cases} \tag{15}$$

A useful quantification of the ovalised geometry of a cylindrical shell is offered by the 'out-of-roundness' tolerance parameter U of EN 1993-1-6 [14], defined as:

$$U = \frac{D_{\max} - D_{\min}}{D_{nom}} \tag{15}$$

where D_{max} and D_{min} are the maximum and minimum deformed diameters at the same cross-section in a cylinder, and D_{nom} is the nominal undeformed diameter. Xu et al. (2017) invoked the original assumptions of Brazier [36] together with additional relationships from Karamanos [37] to show that cylinders under uniform bending attain a 'fully-developed' ovalisation of U_{max} ≈ 0.34 at buckling, a result supported by finite element analysis, and that this result is approximately stable for cylinders longer than Ω > 5. The computed distributions of U at buckling along cylinders of varying length Ω, presented in normalised form from 0 to 1 to allow cylinder of different length to be plotted on the same figure, are shown in Fig. 14. This reflects the relationship shown in Fig. 13, with U peaking at approximately midspan until Ω ≈ 2 but becoming increasingly localised towards the base support with increasing total Ω. Further, the peak ovalisation parameter U_{max} for cylinders under transverse shear does not stabilise as it did under uniform bending to become invariant with further increases in length, and in fact ever longer cylinders appear to undergo increasingly severe pre-buckling ovalisation. However, even for a very long cylinder with Ω = 20, U_{max} does not reach the 'upper bound' of 0.34 suggested by Xu et al. [31], suggesting that a cylinder under transverse shear does not *need* to develop the same severity of cross-sectional distortion to support a moment at approximately the Brazier value (Fig. 12). Fig. 14 also illustrates that

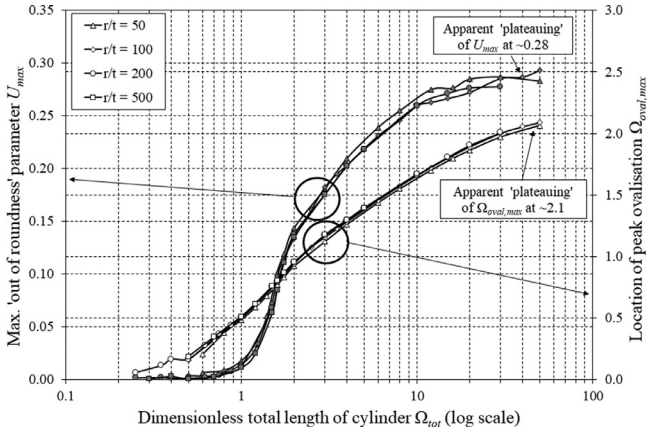

Fig. 15. Variation of the max 'out of roundness' parameter U_{max} and the location of peak ovalisation Ω_{ova} with the total cylinder length (here termed Ω_{tot} for clarity).

cylinders in the 'medium-bending' domain (Ω ≤ 1.6) may also exhibit finite peak ovalisation at midheight, although not sufficient to influence the buckling behaviour.

The above is explored further in Fig. 15 which suggests that the peak ovalisation in fact tends to an asymptotic value of ~0.28 under transverse shear, somewhat below the value of ~0.34 under uniform bending. Lastly, Fig. 15 also illustrates that although the *relative* location of peak ovalisation $\Omega_{oval,max}$ / Ω tends to zero with increasing total cylinder length, the *absolute* location appears to tend to an asymptotic value of $\Omega_{oval,max}$ ≈ 2.1. Thus, it may be anticipated that elastic buckling of a long uniform-thickness cylinder under transverse shear should occur within a length of ~$2.1r\sqrt{(r/t)}$ of the base support. It did not prove feasible to explore cylinders longer than Ω = 50 due to the increasingly severe ill-conditioning of the finite element models and excessive runtimes, and more accurate asymptotic values of U_{max} or $\Omega_{oval,max}$ are not currently available.

7. Imperfection sensitivity of cylinders under transverse shear

A computational investigation of imperfection sensitivity in cylinders under transverse poses a conceptual as well as computational challenge because of the qualitative variation of the critical buckling mode with cylinder length. It has been documented that short cylinders buckling into a shear mode are only mildly sensitive to eigenmode-affine imperfections [11]. Here, a series of GNIAs were first performed for cylinders with r/t= 100 of varying length with an imposed imperfec-

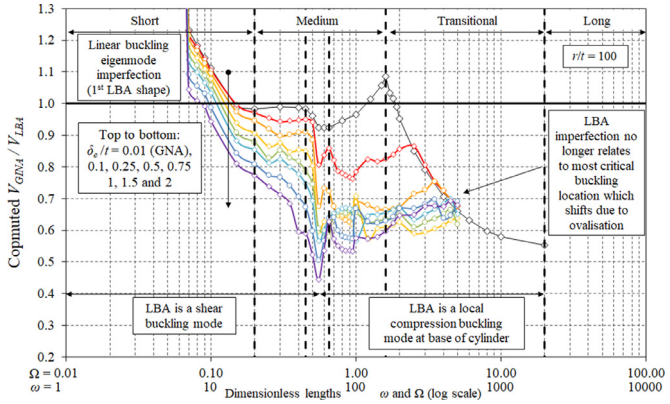

Fig. 16. Computed relationship between the nonlinear elastic buckling resistance V_{GNIA} / V_{LBA} of imperfect cantilever cylinders and the dimensionless length Ω for the linear buckling eigenmode imperfection.

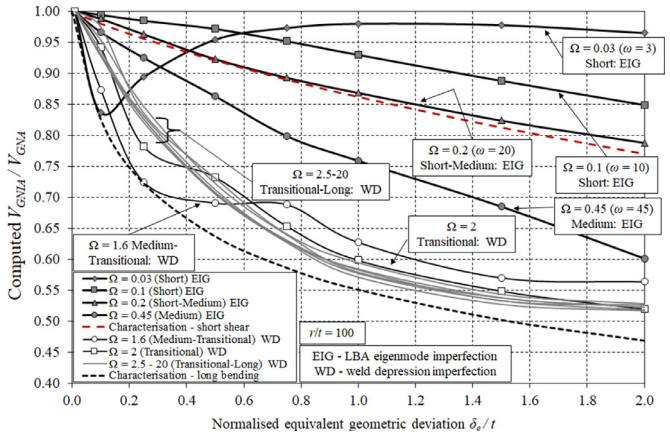

Fig. 17. Computed imperfection sensitivity relationships V_{GNIA} / V_{GNA} at various cylinder lengths for r/t = 100 and both imperfection forms.

tion in the form of the critical LBA eigenmode (see Fig. 6 for examples), illustrated in Fig. 16. Very short cylinders, where shear buckling is restrained by the end boundary condition, duly exhibit an almost total insensitivity to an eigenmode imperfection due to stable nature of the post-buckling equilibrium path (Fig. 8). This is evident in the imperfection sensitivity relationship for ω= 3 in Fig. 17 which shows an approximately stable reduction in buckling resistance of less than 5% across the range of 'equivalent geometric deviations' δ_e/t from 0.5 to 2, despite an initial 'dip' at small amplitudes. By $\omega \approx 7$, the beneficial effect of the end restraint vanishes and the shell may buckle freely into a shear mode, and imperfection sensitivity assumes a 'classical' monotonically-decreasing relationship with δ_e/t. It also becomes more deleterious with further increases in length: the reduction over V_{GNA} is 15%, 22% and 40% at δ_e/t= 2 for ω= 10, 20 and 45 respectively, although still less severe than under uniform meridional compression.

A rather ambiguous GNIA relationship is revealed in the 'medium-interaction' length domain due to the transition from shear to bending-dominated buckling, both in the LBA and GNA behaviour (Figs. 6 and 9). Imperfection sensitivity in the 'medium-bending' domain the relationship is again relatively stable, as both the LBA and GNA buckling modes now coincide to occur at the base of the cylinder. However, the computation of GNIAs was discontinued shortly into the 'transitional' domain where it became evident that the LBA imperfection mode, which in the present system must *always* predict a localised buckle at the base of the cylinder at lengths beyond $\Omega_{z,\theta\text{-}z}$= 0.65 (even for higher modes), became disjoint from the critical buckling location at the most ovalisation cross-section (Figs. 13 and 14) and had an almost entirely negligible

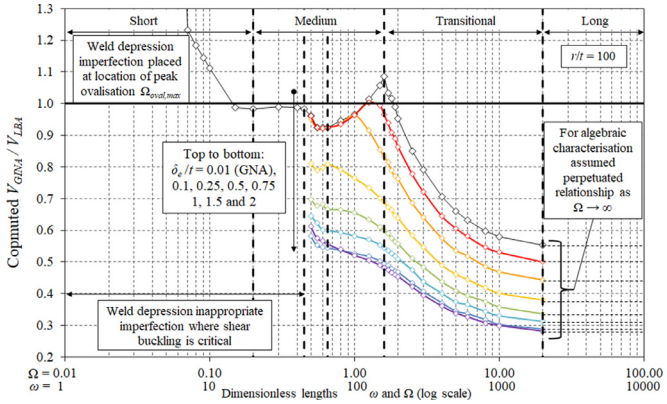

Fig. 18. Computed relationship between the nonlinear elastic buckling resistance V_{GNIA} / V_{LBA} of imperfect cantilever cylinders and the dimensionless length Ω for the weld depression imperfection placed at the location of peak ovalisation $\Omega_{oval,max}$.

effect on the buckling resistance, even at very deep amplitudes. This should serve as a caution to structural analysts attempting to perform GMNIA calculations with only a naïve implementation of the critical linear eigenmode as an imperfection form. The choice of a meaningful imperfection should be made carefully so that it relates to the mechanics of the nonlinear response of the system (see discussion in Sadowski and Rotter [38]).

A second set of GNIAs was performed with a single Rotter and Teng [12] Type 'A' weld depression, defined by the functional form in Eq. (16), placed at the most ovalised location $L_{oval,max}$ as predicted by Eq. (15) on the basis of GNAs. GNIAs with this imperfection form were not performed for cylinders shorter than Ω ≈ 0.5 controlled by shear buckling and for which the eigenmode imperfection proved more critical at the same value of the 'equivalent geometric deviation' δ_e/t. Illustrated in Fig. 18, it is evident that when the weld depression is placed at the most-ovalised location that is critical for buckling in a GNA, its deleterious effect is maximised and effectively invariant with further changes in length (see also the group of curves for 2.5 ≤ Ω ≤ 20 in Fig. 17). GNIAs for very long cylinders with Ω > 20 were not performed.

$$\delta = \delta_0 e^{-w(z)}(\cos w(z) + \sin w(z)) \; where \; w(z) = \frac{\pi}{\lambda}\left|z - L_{oval,\max}\right| \; and \; \lambda \approx 2.44\sqrt{rt} \tag{16}$$

The simple lower-bound relationship in Eq. (17) is offered to capture the imperfection sensitivity of this system across domains governed by either shear or local meridional compression buckling, including the interactive region in-between, aiming to strike a balance between ease of use and realism. Together with the expressions for V_{cr} (approximating V_{LBA}) and $V_{k,per}$ (approximating V_{GNA}) in Eqs. (11) and (14) respectively, these permit a smooth, conservative and closed-form algebraic prediction of the nonlinear global transverse shear resistance of an elastic imperfect uniform-thickness cylindrical shell. Illustrated in Fig. 19, it may be seen that the greatest source of ambiguity in this relationship is in the 'medium' domain due to a messy transition from shear-dominated to bending-dominated behaviour. A synthetic GNIA data set is shown here, constructed by taking the lowest result from either imperfection at the same length and δ_e/t (see Fajuyitan and Sadowski [21] for a similar approach applied to cylinders under uniform bending). The dashed lines show the $V_{k,imp}$ / V_{LBA} characterisation offered by Eq. (17) for various δ_e/t, where it is proposed that the imperfection sensitivity at ω= 20 be perpetuated 'leftwards' for all shear-dominated behaviour in very short cylinders, while that at Ω = 20 be perpetuated 'rightwards' for all bending-dominated behaviour in very long cylinders. An exponential decay is proposed for the 'medium' domain, with an exponent p that

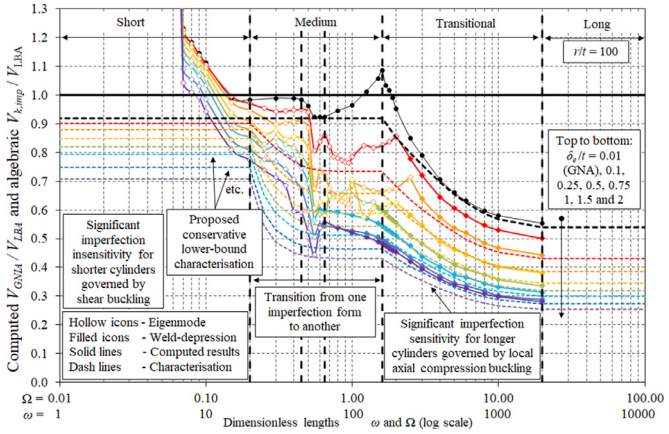

Fig. 19. Computed relationship between the nonlinear elastic buckling resistance V_{GNIA} / V_{LBA} of imperfect cantilever cylinders and the dimensionless length Ω, including a lower-bound transition from between two imperfection forms and a proposed conservative characterisation of the length-dependent imperfection sensitivity.

may be adjusted as desired.

$$\frac{V_{k,imp}}{V_{k,per}} = \frac{1}{1 + x_1 \left(\delta_e / t\right)^{x_2}} \tag{17}$$

where

$$x_i = \begin{cases} a_{z\theta,i} & \Omega \le 20\dfrac{t}{r}\text{(shear)} \\ a_{z,i} + (a_{z\theta,i} - a_{z,i}) e^{-p\left(\Omega - 20\frac{t}{r}\right)} & 20\dfrac{t}{r} < \Omega < 1.6\text{(interaction)} \\ a_{z,i} & \Omega \ge 1.6\text{(bending)} \end{cases}$$

such that $(a_{z\theta,1}, a_{z\theta,2}) = (0.16, 0.9)$, $(a_{z,1}, a_{z,2}) = (0.8, 0.5)$ and $p = 10$.

8. Conclusions

This paper has presented a comprehensive computational investigation into the nonlinear elastic buckling response of both perfect and imperfect clamped cantilever cylindrical shells under global transverse shear. An exhaustive range of practical lengths and slendernesses was covered, from short cylinders which fail by shear buckling to long ones which exhibit local meridional compression buckling influenced by cross-sectional ovalisation, as well as the transitions in-between. Both the geometrically linear and nonlinear responses were studied, the latter for both perfect and imperfect cylinders. It is thought that this paper is the first ever to undertake such a detailed parametric study of this ubiquitous structural system.

Under geometrically linear conditions, the system exhibits four qualitatively distinct length domains, a consequence of the complex interaction between two governing buckling modes and the effect of boundary restraint at very short lengths. However, under geometrically nonlinear conditions, the number of length domains rises to six due to the important influence of pre-buckling ovalisation on longer cylinders dominated by meridional compression buckling. The influence of ovalisation was studied in detail and it is shown that the long elastic cylinders effectively buckle at just below the 'Brazier' reference bending moment at the most ovalised cross-section.

A relatively mild sensitivity to eigenmode-affine imperfections was revealed for short cylinders governed by shear buckling, consistent with the findings of previous authors. However, longer cylinders proved very sensitive to an axisymmetric 'weld depression' imperfection placed at the most ovalised location, also the critical location for meridional compression buckling in the perfect shell. This careful placement has the effect of maximising the damaging effect of these imperfections in long cylinders and making the imperfection sensitivity invariant with length.

The authors have additionally distilled and characterised the phenomena into closed-form algebraic expressions suitable for direct use as design equations. These make use of carefully-chosen dimensionless groups from background theory to enable the relationship to be expressed independently of the slenderness, expressed by the radius to thickness ratio. They have been designed to strike a balance between ease of use and realism, and may be used to obtain a conservative but reasonably realistic estimate of the nonlinear resistance of an elastic imperfect cantilever cylinder. The study forms part of a larger research programme aiming to cover a wide range of classical shell systems and characterise their global behaviour within the framework of Reference Resistance Design [18,24,25]. Extension of the work to material nonlinearity is currently ongoing and will be presented at a later time.

Acknowledgement

This work was partly funded by the UK Engineering and Physical Sciences Research Council (EPSRC)with grant contract EP/N024060/1.

References

[1] Lu SY. Buckling of a cantilever cylindrical shell with a transverse end load. AIAA J 1965;3:2350–1.
[2] Schröder P. Über die Stabilität der querkraftbelasteten dünnwandigen Kreiszylinderschalen. Zeitschrift für Angewandte Mathematik 1972;52:T145–8.
[3] Rotter JM, Sadowski AJ, Chen L. Nonlinear stability of thin elastic cylinders of different length under global bending. Int J Solids Struct 2014;51:2826–39.
[4] Calladine CR. Theory of shell structures. Cambridge: University Press; 1983.
[5] Lundquist EE. Strength tests of thin-walled duralumin cylinders in combined transverse shear and bending. National Advisory Committee for Aeronautics; 1935. Technical Note 523.
[6] Yamaki N. Elastic stability of circular cylindrical shells. Elsevier Science; 1984. North-Holland.
[7] Galletly GD, Błachut J. Plastic buckling of short vertical cylindrical shells subjected to horizontal edge shear loads. ASME J Pressure Vessel Technol 1985;107:101–6.
[8] Michel G, Limam A, Jullien JF. Buckling of cylindrical shells under static and dynamic shear loading. Eng Struct 2000;22:535–43.
[9] Athiannan K, Palaninathan R. Buckling of cylindrical shells under transverse shear. Thin Walled Struct 2004;42:1307–28.
[10] Schmidt H, Winterstetter Th A. Cylindrical shells under shear stresses. In: Buckling of thin metal shells. London: Spon Press; 2004. p. 207–29.
[11] Kokubo K, Nagashima H, Takayanagi M, Mochizuki A. Analysis of shear buckling of cylindrical shells. JSME Int J Mech Mater Eng 1993;36(3):259–66.
[12] Rotter JM, Teng JG. Elastic stability of cylindrical shells with weld depression. ASCE J Struct Eng 1989;115(5):1244–63.
[13] Gettel M, Schneider W. Buckling strength verification of cantilevered cylindrical shells subjected to transverse load using Eurocode 3. J Construct Steel Res 2007;63:1467–78.
[14] EN 1993-1-6 Eurocode 3: Design of steel structures. Part 1-6: Strength and stability of shell structures. Comité Européen de Normalisation 2007 CEN, Brussels.
[15] Schneider W, Thiele R. Eine unerwartete Versagensform bei schlanken windbelasteten Kreiszylinderschalen. Stahlbau 1998;67(11):870–5.
[16] Stamatopoulos GN. Response of a wind turbine subjected to near-fault excitation and comparison with the Greek Aseismic Code provisions. Soil Dyn Earthq Eng 2013;46:77–84.
[17] Michel G, Jullien JF, Rotter JM. Cylindrical shells under global shear loading. In: Buckling of thin metal shells. London: Spon Press; 2004. p. 230–60.
[18] Sadowski AJ, Fajuyitan OK, Wang J. A computational strategy to establish algebraic parameters for the Reference Resistance Design of metal shell structures. Adv Eng Software 2017;109:15–30.
[19] Song CY, Teng JG, Rotter JM. Imperfection sensitivity of thin elastic cylindrical shells to partial axial compression. Int J Solids Struct 2004;41(24-25):7155–80.
[20] Chen L, Doerich C, Rotter JM. A study of cylindrical shells under global bending in the elastic-plastic range. Steel Constr Des Res 2008;1(1):59–65.
[21] Fajuyitan O.K., Sadowski A.J. "Imperfection sensitivity in cylindrical shells under uniform bending" *Under Review*.
[22] Pircher M, Berry PA, Ding X, Bridge RQ. The shape of circumferential weld-induced imperfections in thin-walled steel silos and tanks. Thin Walled Struct 2001;39(12):999–1014.
[23] Fajuyitan OK, Sadowski AJ, Wadee MA, Rotter JM. Nonlinear behaviour of short elastic cylindrical shells under global bending. Thin Walled Struct 2018;124:574–87.
[24] Rotter JM. The new method of reference resistance design for shell structures. In: Proceedings of the International Colloquium on Stability and Ductility of Steel Structures (SDSS 2016); 2016. p. 623–30. May 30 – June 1.
[25] EN 1993-1-6:A1. Eurocode 3: Design of steel structures. Part 1-6: Strength and stability of shell structures. Amendment A1. CEN, Brussels: Comité Européen de Normalisation; 2017.
[26] ABAQUS. ABAQUS v. 6.14-2" Commercial FE Software and Documentation. Providence, RI, USA: Dassault Systèmes, Simulia Corporation; 2014.

[27] Sadowski AJ, Rotter JM. On the relationship between mesh and stress field orientations in linear stability analyses of thin plates and shells. Finite Elem Anal Des 2013;73:42–54.
[28] Matsuura S, Nakamura H, Kokubo K, Ogiso S, Ohtsubo H. Shear-bending buckling analyses of fast breeder reactor main vessels. Nucl Eng Des 1995;153:305–17.
[29] Schneider W, Thiele R. Tragfähigkeit schlanker wind-belasteter Kreiszylinderschalen. Stahlbau 1998;67(6):434–41.
[30] Timoshenko SP, Gere JM. Theory of elastic stability. 2nd ed. New York, USA: McGraw-Hill; 1961.
[31] Xu Z, Gardner L, Sadowski AJ. Nonlinear stability of elastic elliptical cylindrical shells under uniform bending. Int J Mech Sci 2017;128-129:593–606.
[32] Timoshenko SP. On the correction factor for shear of the differential equation for transverse vibrations of bars of uniform cross-section. Philosoph Mag 1921:744.
[33] Cowper GR. The shear coefficient in Timoshenko's Beam Theory. ASME J Appl Mech 1966;33(2):335–40.
[34] ECCS EDR 5 (2013). European recommendations for steel construction: buckling of shells 5th ed. 2nd Imp., Eds. Rotter J.M., & Schmidt H., European convention for constructional steelwork Brussels.
[35] Sadowski AJ, Rotter JM. Steel silos with different aspect ratios: I – behaviour under concentric discharge. J Constr Steel Res 2011;67:1537–44.
[36] Brazier LG. On the flexure of thin cylindrical shells and other 'thin' sections. Proc. R Soc 1927;116:104–14 Series A.
[37] Karamanos S. Bending instabilities of elastic tubes. Int J Solids Struct 2002;39:2059–85.
[38] Sadowski AJ, Rotter JM. Exploration of novel geometric imperfection forms in buckling failures of thin-walled metal silos under eccentric discharge. Int J Solids Struct 2013;50:781–94.